rosine phosphorylation sites on IRS-1/2 await clarification.

In contrast to the liver, the muscles of Zucker fatty rats showed no apparent shift in the relation between binding of IRS-1/2 to the p85α regulatory subunit and PI 3-kinase activity.

High-fat Diet Induces Tissue-Specific Alteration in Insulin Signaling Numerous studies have now confirmed that insulin action is impaired in liver, muscle and adipose tissues of rats maintained on a high-fat diet. For example, basal hepatic glucose production is increased in such rats, and insulin-induced suppression of this glucose production is impaired. With a high-fat diet, glycogen synthesis decreases in both muscle and liver, and insulin-induced glucose uptake and GLUT4 translocation to the plasma membrane are reduced in both muscle and adipose tissues. It is clear then that excessive dietary fat consumption can lead to insulin resistance in all three tissues.

The levels of IRS-1/2 protein in hepatic and muscle tissues of rats on a high-fat diet were found to be similar to those of control rats. In contrast, levels of IRS-1/2 in the epididymal fat were decreased to 55% and 65% of those in control rats.[37] Impaired insulin-stimulated tyrosine phosphorylation of IRS-1/2 has been observed in several diabetic animal models, and there was a tendency for tyrosine phosphorylation of IRS-1/2 to be decreased in the livers of rats on high-fat diets, but the difference was not statistically significant. Insulin-evoked tyrosine phosphorylation of IRS-1/2 in muscle was lower in fat-fed rats than in controls, however, and, the suppressive effect of high fat was even more pronounced in the epididymal fat. However, surprisingly, both basal and insulin-stimulated levels of IRS-1/2-bound p85α were increased in the livers of rats on high-fat diets, although phosphorylation of IRS-1/2 was unchanged. In muscle, by contrast, insulin-stimulated levels of IRS-1/2-bound p85α in rats on high-fat diets were significantly decreased to 78% and 68% of the control levels, while in the epididymal fat, the levels were down to 74% and 53% of the control levels.

The insulin-induced elevation of IRS-1/2-bound p85α seen in the livers of rats on a high-fat diet resulted in a 2-fold increase in PI 3-kinase activity, whereas the declines in IRS-1/2-bound p85α in muscle and epididymal fat resulted in concomitant, significant declines PI 3-kinase activity.

Levels of IRS-1/2 protein were unaltered in the muscles of rats fed a high-fat diet, although their phosphorylation was impaired. It is likely, therefore, that the reduced p85α binding and PI 3-kinase activity seen in the muscle tissues of rats fed a high-fat diet resulted from decreased tyrosine phosphorylation of IRS-1/2. In the case of epididymal fat, IRS-1/2 expression was reduced by 30—40% as compared to the control, which in turn led to reduced levels of tyrosine phosphorylation, reduced binding to p85α, and reduced PI 3-kinase activity. In contrast to muscle, therefore, insulin signaling is impaired mainly at the level of IRS-1/2 expression in the adipose tissues of fat-fed rats.

Hepatic expression of IRS-1/2 was not significantly altered in fat-fed rats, nor was expression of PI 3-kinase; tyrosine phosphorylation of IRS-1/2 was altered only slightly; and increased PI 3-kinase resulted from significantly augmented binding of IRS-1/2 to p85α. The fact that PI 3-kinase activation was significantly enhanced in the livers of rats fed a high-fat diet clearly indicates that such a diet causes hepatic

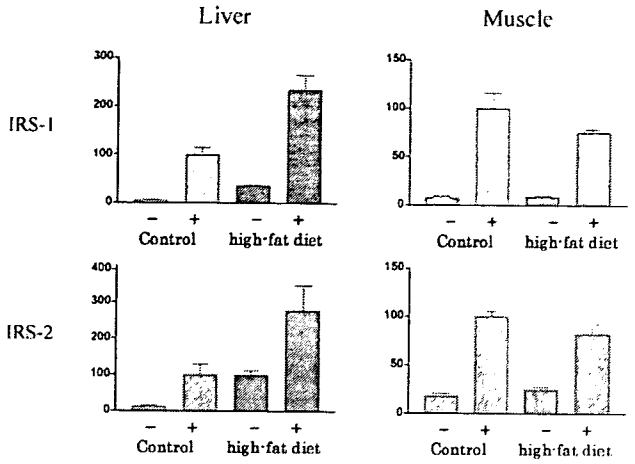

Fig. 3. PI 3-Kinase Activity in Liver and Muscle of SD Rats Maintained on High-Fat Diets

insulin resistance by a mechanism other than those underlying decreased insulin sensitivity in muscle and adipose tissues.

IRS-1/2 each contain approximately 20 putative tyrosine phosphorylation sites, only four of which are in the Y(M/X)XM motif responsible for the interaction with PI 3-kinase regulatory subunits. IRS-1/2 also contains more than 30 potential serine/threonine phosphorylation sites for casein kinase II, protein kinase C, MAP kinase and cdc2, as well as phosphorylation sites for cAMP- and cGMP-dependent protein kinases. It seems reasonable, therefore, to suggest that in rats on a high-fat diet, a change in the phosphorylation state at one or more of those other sites might upregulate the phosphorylation of specific hepatic tyrosine residues, thereby augmenting p85α binding to IRS-1/2, while phosphorylation of other tyrosine residues, or at least those efficiently recognized by the anti-phosphotyrosine antibody used in our assay, are unaffected. Alternatively, the possibility that IRS-1/2 binding to p85α is increased by an as yet unknown modification of the p85α protein—*e.g. via* serine/threonine phosphorylation(s)—cannot be excluded.

It was especially interesting to us that insulin-stimulated PI 3-kinase activity was severely impaired in the livers of other obese diabetic rodent models, such as ob/ob mice[38] and Zucker fatty rats,[36] while being enhanced in the livers of rats fed a high fat diet. The effects of a high-fat diet on insulin-stimulated PI 3-kinase activation were thus clearly opposite those of obesity induced by general overeating (*i.e.* obesity due to leptin system dysfunction), suggesting that in fat-fed rats impaired insulin action may originate downstream from PI 3-kinase activation.

Hyperglycemia-Induced Alteration in Insulin Signaling Hyperglycemia is believed to contribute to the development of peripheral insulin resistance associated with both type 1 and type 2 diabetes. Many reports support the significant correlation between blood glucose level and peripheral insulin resistance. To determine the molecular mechanism underlying hyperglycemia-induced insulin resistance in skeletal muscles, post-receptor insulin-signaling events were assessed in skeletal muscles of neonatally streptozotocin-treated diabetic rats[39] and Zucker diabetic rats.[40] In soleus muscles isolated from diabetic rats, insulin-stimulated 2-deoxyglucose

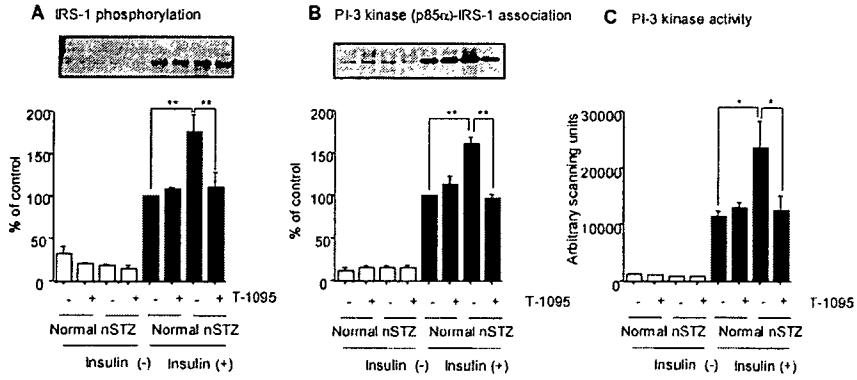

Fig. 4. Tyrosine Phosphorylation (A) of IRS-1, and Amount (p85α) (B) and Activity (C) of PI 3-kinase Associated with IRS-1 in Basal and Insulin-Stimulated Skeletal Muscle of Normal and nSTZ Rats with or without T-1095-Treatment

The proteins immunoprecipitated with anti-IRS-1 were subjected to SDS-PAGE followed by immunoblotting with anti-phosphorylated tyrosine (4G10) (A) or anti-p85α (B), or determination of PI 3-kinase activity (C). (A) A representative autoradiograph (upper) and the quantified data (lower) of tyrosine phosphorylation of IRS-1. (B) A representative autoradiograph (upper) and the quantified data (lower) of p85α associated with IRS-1. (C) PI 3-kinase activity associated with IRS-1. Results are expressed as the mean±S.E. for three animals. $*p<0.05$, $**p<0.01$.

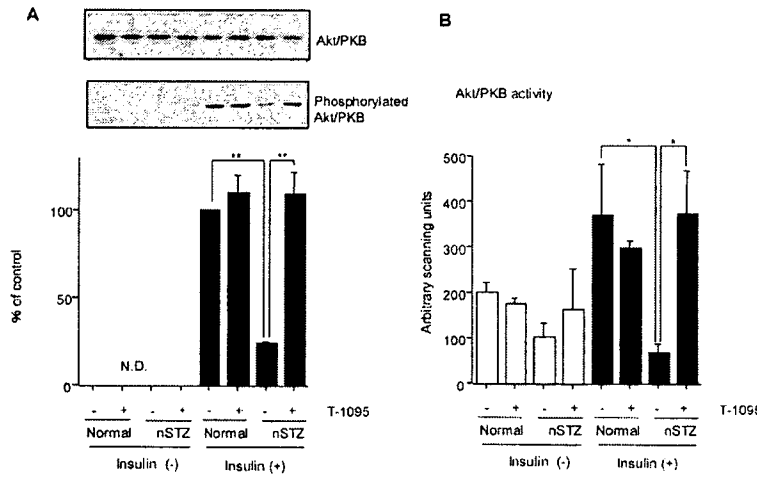

Fig. 5. The Protein Expression, Phosphorylation (Ser473) (A) and Activity (B) of Akt/PKB in Basal and Insulin-Stimulated Skeletal Muscle of Normal and nSTZ Rats with or without T-1095-Treatment

The total lysate was subjected to SDS-PAGE followed by immunoblotting with anti-Akt/PKB or anti-phosphorylated (Ser473) Akt/PKB (A). Equal amounts of muscle protein were immunoprecipitated with anti-Akt/PKB followed by determination of Akt/PKB activity (B). (A) Representative autoradiographs of Akt/PKB (upper) and phosphorylated Akt/PKB (middle), and the quantified data.

uptake, glucose oxidation and lactate release were all significantly decreased as compared with those of normal rats. Similarly, insulin-induced phosphorylation and activation of Akt/protein kinase B (PKB) and GLUT4 translocation were severely impaired. However, the upstream signals including phosphorylation of the insulin receptor and the insulin receptor substrate (IRS) -1/2, as well as PI 3-kinase activity associated with IRS-1/2, were enhanced. The amelioration of hyperglycemia by T-1095, a Na^+-glucose transporter inhibitor,[41] normalized the reduced insulin sensitivity in the soleus muscle, and the impaired insulin-stimulated Akt/PKB phosphorylation and activity. In addition, the enhanced PI 3-kinase activation and phosphorylation of the insulin receptor and IRS-1/2 were normalized. These results suggest that sustained hyperglycemia impairs the insulin-signaling steps between PI 3-kinase and Akt/PKB, and that impaired Akt/PKB activity underlies hyperglycemia-induced insulin resistance in skeletal muscle.

Salt-Sensitive or Angiotensin II-Related Hypertension Induces Insulin Resistance with Enhances in Insulin Signaling It is well-known that excessive salt intake elevates blood pressure and that hypertension often coexists with insulin resistance. However, the contribution of salt intake to the development of insulin resistance has yet to be clarified. We have investigated the molecular mechanism underlying insulin resistance in salt-sensitive rat models such as high-salt diet fed Sprague-Dawley rats,[42] Dahl salt-sensitive rats[43] and chronically angiotensin II (AII)-infused rats.[44] Importantly, the common observations in these rats were that despite that their being insulin-resistant, insulin-induced tyrosine phosphorylation of the insulin receptor and insulin receptor substrates, activation of phosphatidylinositol 3-kinase, and phosphorylation of Akt were all enhanced. Thus, the molecular mechanism underlying insulin resistance related to salt sensitive hypertension is unique, since many other factors causing insulin resistance such as obesity suppress an early insulin signaling step that is between the insulin receptor and PI 3-kinase activation. Interestingly, potassium (8%

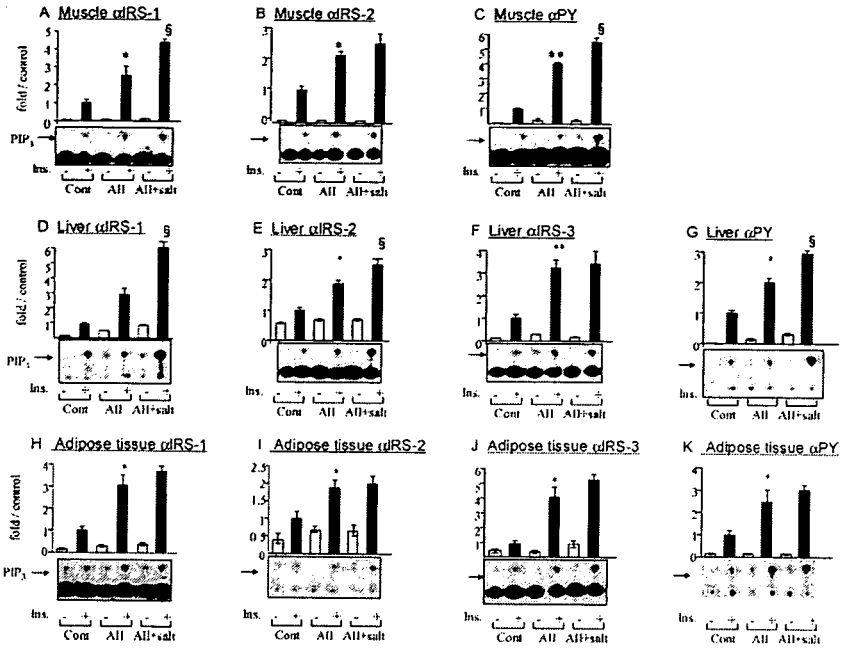

Fig. 6. Insulin-Stimulated PI 3-Kinase Activation in Skeletal Muscle, Liver and Fat of Angiotensin II-Infused Rats

Rats were anesthetized, and 4 ml of normal saline with or without 10^{-5} mol/l human insulin were then injected. Livers and hindlimb muscles were removed and homogenized (n=3 in each group). The lysates were subjected to immunoprecipitation with anti-IRS-1, anti-IRS-2, anti-IRS-3 or anti-phosphotyrosine antibodies followed by protein A-Sepharose 4FF. PI 3-kinase activities in the immunoprecipitates were assayed. The bar represents the average PI 3-kinase activity of three independently performed experiments. Representative spots of PI(3)P are shown. Data are means±S.E. *$p<0.05$ and **$p<0.01$ with the controls and §$p<0.05$ compared with the AII group in the presence of insulin.

KCl) supplementation ameliorated the changes in insulin sensitivity in Dahl-S rats fed a high-salt diet, associated with a slight, but significant, decrease in blood pressure.

In addition, chronic AII infusion induced plasma cholesterylester hydroperoxide accumulation indicating increased oxidative stress, while treatment with tempol normalized plasma hydroperoxide levels in AII-infused rats. In addition, the tempol treatment normalized insulin resistance in AII-infused rats, as evidenced by a decreased glucose infusion rate in hyperinsulinemic euglycemic clamp study and decreased insulin-induced glucose uptake into isolated skeletal muscle, as well as enhanced insulin-induced PI 3-kinase activation as compared to the control rats. Thus, the mechanism underlying AII or high-salt diet induced insulin resistance may be increased oxidative stress, at least in part. Though further study is necessary to fully elucidate these mechanisms, our findings also suggest the importance of the development of new therapeutic approaches (for example, potassium supplementation or anti-oxidant administration) for patients with insulin resistance and hypertension.

REFERENCES

1) White M. F., Kahn C. R., *J. Biol. Chem.*, **269**, 1—4 (1994).
2) Ogihara T., Isobe T., Ichimura T., Taoka M., Funaki M., Sakoda H., Onishi Y., Inukai K., Anai M., Fukushima Y., Kikuchi M., Yazaki Y., Oka Y., Asano T., *J. Biol. Chem.*, **272**, 25267—25274 (1997).
3) Okada T., Kawano Y., Sakakibara T., Hazeki O., Ui M., *J. Biol. Chem.*, **269**, 3568—3573 (1994).
4) Katagiri H., Asano T., Ishihara H., Inukai K., Shibasaki Y., Kikuchi M., Yazaki Y., Oka Y., *J. Biol. Chem.*, **271**, 16987—16990 (1996).
5) Martin S. S., Haruta T., Morris A. J., Klippel A., Williams L. T., Olefsky J. M., *J. Biol. Chem.*, **271**, 17605—17608 (1996).
6) Gabbay R. A., Sutherland C., Gnudi L., Kahn B. B., O'Brien R. M., Granner D. K., Flier J. S., *J. Biol. Chem.*, **271**, 1890—1897 (1996).
7) Shepherd P. R., Nave B. T., Siddle K., *Biochem. Soc. Trans.*, **23**, 202S (1995).
8) Sutherland C., O'Brien R. M., Granner D. K., *J. Biol. Chem.*, **270**, 15501—15506 (1995).
9) Inoue G., Cheatham B., Emkey R., Kahn C. R., *J. Biol. Chem.*, **273**, 11548—11555 (1998).
10) Kido Y., Burks D. J., Withers D., Bruning J. C., Kahn C. R., White M. F., Accili D., *J. Clin. Invest.*, **105**, 199—205 (2000).
11) Songyang Z., Shoelson S. E., Chaudhuri M., Gish G., Pawson T., Haser W. G., King F., Roberts T., Ratnofsky S., Lechleider R. J., Neel B. G., Birge R. B., Fajardo J. E., Chou M. M., Hanafusa H., Schaffhausen B., Cantley L. C., *Cell*, **72**, 767—778 (1993).
12) Otsu M., Hiles I., Gout I., Fry M. J., Ruiz-Larrea F., Panayotou G., Thompson A., Dhand R., Hsuan J., Totty N., Smith A. D., Morgan S. J., Courtneidge S. A., Parker P. J., Waterfield M. D., *Cell*, **65**, 91—104 (1991).
13) Gout I., Dhand R., Panayotou G., Fry M. J., Hiles I., Otsu M., Waterfield M. D., *Biochem. J.*, **288**, 395—405 (1992).
14) Pons S., Asano T., Glasheen E., Miralpeix M., Zhang Y., Fisher T. L., Myers M. G., Sun X. J., White M. F., *Mol. Cell. Biol.*, **15**, 4453—4465 (1995).
15) Inukai K., Anai M., Breda E. V., Hosaka T., Katagiri H., Funaki M., Fukushima Y., Ogiwara T., Yazaki Y., Kikuchi M., Oka Y., Asano T., *J. Biol. Chem.*, **271**, 5317—5320 (1996).
16) Antonetti D., Algenstaedt P., Kahn C. R., *Mol. Cell. Biol.*, **16**, 2195—2203 (1996).
17) Inukai K., Funaki M., Ogihara T., Katagiri H., Kanda A., Anai M., Fukushima Y., Hosaka T., Suzuki M., Shin B. C., Takata K., Yazaki Y., Kikuchi M., Oka Y., Asano T., *J. Biol. Chem.*, **272**, 7873—7882 (1997).
18) Albert S., Twardzik T., Heisenberg M., Schneuwly S., *Gene*, **198**, 181—189 (1997).
19) Asano T., Kanda A., Katagiri H., Nawano M., Ogihara T., Inukai K., Anai M., Fukushima Y., Yazaki Y., Kikuchi M., Hooshmand-Rad R., Heldin C. H., Oka Y., Funaki M., *J. Biol. Chem.*, **275**, 17671—17676 (2000).
20) Stephens L., Anderson K., Stokoe D., Erdjument-Bromage H., Painter G. F., Holmes A. B., Gaffney P. R., Reese C. B., McCormick F., Tempst P., Coadwell J., Hawkins P. T., *Science*, **279**, 710—714 (1998).
21) Anderson K. E., Coadwell J., Stephens L. R., Hawkins P. T., *Curr.*

Biol., **8**, 684—691 (1998).
22) Singh S. S., Chauhan A., Brockerhoff H., Chauhan V. P., *Biochem. Biophys. Res. Commun.*, **195**, 104—112 (1993).
23) Klarlund J. K., Guilherme A., Holik J. J., Virbasius J. V., Chawla A., Czech M. P., *Science*, **275**, 1927—1930 (1997).
24) Venkateswarlu K., Oatey P. B., Tavare J. M., Cullen P. J., *Curr. Biol.*, **8**, 463—466 (1998).
25) Rameh L. E., Arvidsson A. K., Carraway K. L., 3rd., Couvillon A. D., Rathbun G., Crompton A., VanRenterghem B., Czech M. P., Ravichandran K. S., Burakoff S. J., Wang D. S., Chen C. S., Cantley L. C., *J. Biol. Chem.*, **272**, 22059—22066 (1997).
26) Sander E. E., van Delft S., ten Klooster J. P., Reid T., van der Kammen R. A., Michiels F., Collard J. G., *J. Cell. Biol.*, **143**, 1385—1398 (1998).
27) Rameh L. E., Chen C. S., Cantley L. C., *Cell*, **83**, 821—830 (1995).
28) Salim K., Bottomley M. J., Querfurth E., Zvelebil M. J., Gout I., Scaife R., Margolis R. L., Gigg R., Smith C. I., Driscoll P. C., Waterfield M. D., Panayotou G., *EMBO J.*, **15**, 6241—6250 (1996).
29) Bae Y. S., Cantley L. G., Chen C. S., Kim S. R., Kwon K. S., Rhee S. G., *J. Biol. Chem.*, **273**, 4465—4469 (1998).
30) Lambrechts A., Verschelde J. L., Jonckheere V., Goethals M., Vandekerckhove J., Ampe C., *EMBO J.*, **16**, 484—494 (1998).
31) Alessi D. R., James S. R., Downes C. P., Holmes A. B., Gaffney P. R., Reese C. B., Cohen P., *Curr. Biol.*, **7**, 261—269 (1997).
32) Sarbassov D. D., Guertin D. A., Ali S. M., Sabatini D. M., *Science*, **307**, 1098—1101 (2005).
33) Whiteman E. L., Cho H., Birnbaum M. J., *Trends Endocrinol. Metab.*, **13**, 444—451 (2002).
34) Cho H., Mu J., Kim J. K., Thorvaldsen J. L., Cho Q., Crensshaw E. B., 3rd., Kaestner K. H., Bartlomei M. S., Shulman G. I., Birnbaum M. J., *Science*, **292**, 1728—1731 (2001).
35) Hotamisligil G. S., Budavari A., Murray D., Spiegelman B. M., *J. Clin. Invest.*, **94**, 1543—1549 (1994).
36) Anai M., Funaki M., Ogihara T., Terasaki J., Inukai K., Katagiri H., Fukushima Y., Yazaki Y., Kikuchi M., Oka Y., Asano T., *Diabetes*, **47**, 13—23 (1998).
37) Anai M., Funaki M., Ogihara T., Kanda A., Onishi Y., Sakoda H., Inukai K., Nawano M., Fukushima Y., Yazaki Y., Kikuchi M., Oka Y., Asano T., *Diabetes*, **48**, 158—169 (1999).
38) Folli F., Saad M. J., Backer J. M., Kahn C. R., *J. Clin. Invest.*, **92**, 1787—1794 (1993).
39) Nawano M., Ueta K., Oku A., Arakawa K., Saito A., Funaki M., Anai M., Kikuchi M., Oka Y., Asano T., *Biochem. Biophys. Res. Commun.*, **266**, 252—256 (1999).
40) Nawano M., Oku A., Ueta K., Umebayashi I., Ishirahara T., Arakawa K., Saito A., Anai M., Kikuchi M., Asano T., *Am. J. Physiol. Endocrinol. Metab.*, **278**, E535—E543 (2000).
41) Oku A., Ueta K., Arakawa K., Ishihara T., Nawano M., Kuronuma Y., Matsumoto M., Saito A., Tsujihara K., Anai M., Asano T., Kanai Y., Endou H., *Diabetes*, **48**, 1794—1800 (1999).
42) Ogihara T., Asano T., Ando K., Chiba Y., Sekine N., Sakoda H., Anai M., Onishi Y., Fujishiro M., Ono H., Shojima N., Inukai K., Fukushima Y., Kikuchi M., Fujita T., *Diabetes*, **50**, 573—583 (2001).
43) Ogihara T., Asano T., Ando K., Sakoda H., Anai M., Shojima N., Ono H., Onishi Y., Fujishiro M., Abe M., Fukushima Y., Kikuchi M., Fujita T., *Hypertension*, **40**, 83—89 (2002).
44) Ogihara T., Asano T., Ando K., Chiba Y., Sakoda H., Anai M., Shojima N., Ono H., Onishi Y., Fujishiro M., Katagiri H., Fukushima Y., Kikuchi M., Noguchi N., Aburatani H., Komuro I., Fujita T., *Hypertension*, **40**, 872—879 (2002).

AMPK Mediates Autophagy during Myocardial Ischemia *in vivo*

Hiromitsu Takagi[1], Yutaka Matsui[1], Shinichi Hirotani[1], Xueping Qu[2], Maha Abdellatif[1], Hideyuki Sakoda[3], Tomoichiro Asano[4], Beth Levine[2], and Junichi Sadoshima[1]

[1]Cardiovascular Research Institute, Department of Cell Biology and Molecular Medicine, University of Medicine and Dentistry of New Jersey, New Jersey Medical School, Newark, New Jersey, USA

[2]Departments of Internal Medicine and Microbiology, University of Texas Southwestern Medical Center, Dallas, Texas, USA

[3]Depertment of Internal Medicine, Graduate School of Medicine, University of Tokyo, Tokyo, Japan

[4]Division of Molecular Medical Science, Programs for Biomedical Research, Hiroshima University, Hiroshima, Japan

Running Title: Signaling Mechanisms of Autophagy in the Heart

Corresponding Author: Junichi Sadoshima, Cardiovascular Research Institute, UMDNJ, 185 South Orange Avenue, MSB G-609, Newark, NJ 07103, USA. Phone: (973) 972-8619; E-mail: Sadoshju@umdnj.edu.

Abstract

We have recently shown that autophagy is induced by ischemia and reperfusion in the mouse heart *in vivo*. Ischemia stimulates autophagy through an AMP activated protein kinase (AMPK)-dependent mechanism, whereas reperfusion after ischemia stimulates autophagy through a Beclin 1-dependent but AMPK-independent mechanism. Autophagy plays distinct roles during ischemia and reperfusion: autophagy may be protective during ischemia, whereas it may be detrimental during reperfusion. We will discuss the role of AMPK in mediating autophagy during myocardial ischemia *in vivo*.

Autophagy is a major mechanism for degrading long-lived cytosolic proteins and is the only known pathway for degrading organelles[1]. Autolysosomal degradation of membrane lipids and proteins generates free fatty acids and amino acids, which can then be reused to maintain mitochondrial ATP production and ribosomal protein synthesis.[2] Autophagy is also activated in order to remove damaged organelles and stimulate phagocytic clearance of apoptotic cells.[3] Although the presence of autophagy has been shown in the heart, whether autophagy is salutary or detrimental for the heart remains unknown *in vivo*. We used a mouse model of myocardial ischemia/reperfusion in order to elucidate the functional roles of autophagy in pathologically relevant conditions in the heart.

In our model, myocardial ischemia (20 min) induced increases in autophagosome formation and, after reperfusion, the number of autophagosomes was further increased, [4] confirming the observation made by Decker more than 25 years ago.[5] In our mouse model of ischemia/reperfusion, the cellular ATP content decreases with ischemia and rapidly recovers after reperfusion, causing autophagosome formation to be stimulated

serially, in two distinct conditions, namely energy-starved and energy-unstarved conditions.

AMP activated protein kinase (AMPK) belongs to a conserved family of protein kinases activated by ATP depletion and consequent AMP accumulation. AMPK plays an important role in regulating both fatty acid and glucose metabolism.[6] The yeast homolog, the sucrose nonfermenting protein 1 (Snf1)/Snf4 complex mediates autophagy during starvation, thereby mediating cell adaptation to a glucose-free environment. [7] In mammals, ATP depletion inhibits mammalian target of rapamycin (mTOR) through activation of AMPK and subsequent phosphorylation of tuberous sclerosis complex 2 (TSC2) [8]. Since mTOR negatively regulates autophagy[9], the AMPK-mTOR pathway has been proposed to be an important regulator of autophagy in response to starvation [10, 11]. However, whether AMPK is involved in mediating autophagy has not been shown *in vivo*.

During myocardial ischemia, a rapid drop in intracellular ATP leads to the activation of AMPK. Autophagosomal formation, in response to myocardial ischemia, was decreased in dominant negative AMPK (DN-AMPK) overexpression mice, suggesting that endogenous AMPK plays an important role in mediating autophagy during myocardial ischemia.[4] During myocardial ischemia, the ATP content in the heart was lower, LV end-diastolic pressure, an index of cardiac dysfunction, was higher, and release of creatine kinase and lactate dehydrogenase, an index of myocardial injury, was greater in the DN-AMPK mice compared with control mice. [12, 13] Our new experiment showed that the size of myocardial infarction after extended ischemia (90 min) was greater in DN-AMPK mice than in wild type mice (**Figure 1**). These results suggest that the induction of autophagy by AMPK may contribute to the preservation of ATP content

as well as promotion of cell survival in the ischemic heart. It should be noted, however, that the activation of AMPK enhances ATP production through multiple mechanisms, including increases in glucose uptake, glycolysis, and fatty acid oxidation.[6] The contribution of autophagy to the overall actions of AMPK in the ischemic heart remains to be identified.

Cultured cardiac myocytes develop autophagy in response to glucose and amino acid deprivation. [4] Our preliminary results suggest that DN-AMPK inhibits autophagy by glucose deprivation, but not by amino acid deprivation, indicating that the involvement of AMPK in the induction of autophagy is stimulus-specific.

Activation of AMPK causes phosphorylation of TSC2, thereby leading to inhibition of mTOR.[8] In anoxic cardiac myocytes, however, activation of AMPK leads to an inhibition of protein synthesis through phosphorylation of eukaryotic elongation factor-2 (eEF2) rather than by the inhibition of mTOR.[14] In fact, despite significant activation of AMPK by ischemia, we were unable to observe a significant drop of p70 S6 kinase (p70S6K) phosphorylation by ischemia *in vivo*, suggesting that the activity of mTOR may not be significantly affected by myocardial ischemia *in vivo*.[4] Since eEF2 kinase, which phosphorylates eEF2, regulates autophagy [15], ischemia-induced autophagy may be mediated through the AMPK-eEF2 kinase pathway rather than through the AMPK-induced inhibition of mTOR. AMPK may also stabilize p27 through phosphorylation, which in turn mediates autophagy. [16] In yeast, *SNF1* regulates two genes involved in autophagy, namely *APG1* and *APG13* , and autophagy critically regulates the maintenance of glycogen levels. [7] Since the AMPK $\alpha 2$ subunit contains a

putative nuclear localization signal [6], it is possible that DN-AMPK has direct effects upon the nuclear actions of AMPK, namely transcription of genes involved in autophagy.

Since AMPK is rapidly inactivated during reperfusion, it is unlikely that increases in autophagy during the reperfusion phase continues to be mediated by AMPK-dependent mechanisms.[4] In our model, autophagosomal formation during the reperfusion phase was critically mediated by Beclin1-dependent mechanisms. Furthermore, both apoptosis and the size of the myocardial infarction during the reperfusion phase were reduced in *beclin1*+/- mice, suggesting that autophagy during the reperfusion phase may be detrimental.[4] These results suggest that autophagy, in the presence or absence of energy starvation, could be mediated by distinct signaling mechanisms and have distinct functional significance (**Figure 2**).

The question then arises should AMPK or autophagy be stimulated in situations such as chest pain due to myocardial ischemia? Based upon our previous studies, [4] stimulation of energy salvaging mechanisms during ischemia, including AMPK and autophagy, should be salutary. Controversy exists as to whether the stimulation of AMPK is beneficial for patients with myocardial ischemia, since the stimulation of fatty acid metabolism by AMPK could reduce glucose oxidation and make cardiac metabolism during ischemia less efficient.[17] Therefore, the therapeutic potential of AMPK during ischemia should be evaluated with caution. An alternative strategy to AMPK stimulation would be the direct stimulation of the autophagy machinery. In order to find a better strategy for cardioprotection based upon modulation of autophagy, however, the functional role of autophagy during myocardial ischemia/reperfusion should be defined using a method that regulates autophagy in a more specific and timely manner.

Acknowledgement

We thank Drs. Noboru Mizushima (Tokyo Medical Dental University) and Rong Tian (Brigham and Women's Hospital) for providing us with GFP-LC3 mice and DN-AMPK mice, respectively, and Lauren Danridge for critical reading of the manuscript. This work was supported by U.S. Public Health Service Grants HL59139, HL67724, HL67727, HL69020, and HL73048 and by American Heart Association 0340123N.

References

1. Klionsky DJ, Ohsumi Y. Vacuolar import of proteins and organelles from the cytoplasm. *Annu Rev Cell Dev Biol.* 1999;15:1-32.

2. Lum JJ, DeBerardinis RJ, Thompson CB. Autophagy in metazoans: cell survival in the land of plenty. *Nat Rev Mol Cell Biol.* 2005;6:439-448.

3. Qu X, Zou Z, Sun Q, Luby-Phelps K, Cheng P, Hogan RN, Gilpin C, Levine B. Autophagy gene-dependent clearance of apoptotic cells during embryonic development. *Cell.* 2007;128:931-946.

4. Matsui Y, Takagi H, Qu X, Abdellatif M, Sakoda H, Asano T, Levine B, Sadoshima J. Distinct roles of autophagy in the heart during ischemia and reperfusion: roles of AMP-activated protein kinase and Beclin 1 in mediating autophagy. *Circ Res.* 2007;100:914-922.

5. Decker RS, Wildenthal K. Lysosomal alterations in hypoxic and reoxygenated hearts. I. Ultrastructural and cytochemical changes. *Am J Pathol.* 1980;98:425-444.

6. Arad M, Seidman CE, Seidman JG. AMP-activated protein kinase in the heart: role during health and disease. *Circ Res.* 2007;100:474-488.

7. Wang Z, Wilson WA, Fujino MA, Roach PJ. Antagonistic controls of autophagy and glycogen accumulation by Snf1p, the yeast homolog of AMP-activated protein kinase, and the cyclin-dependent kinase Pho85p. *Mol Cell Biol.* 2001;21:5742-5752.

8. Inoki K, Corradetti MN, Guan KL. Dysregulation of the TSC-mTOR pathway in human disease. *Nat Genet.* 2005;37:19-24.

9. Noda T, Ohsumi Y. Tor, a phosphatidylinositol kinase homologue, controls autophagy in yeast. *J Biol Chem.* 1998;273:3963-3966.

10. Meley D, Bauvy C, Houben-Weerts JH, Dubbelhuis PF, Helmond MT, Codogno P, Meijer AJ. AMP-activated protein kinase and the regulation of autophagic proteolysis. *J Biol Chem.* 2006;281:34870-34879.

11. Samari HR, Seglen PO. Inhibition of hepatocytic autophagy by adenosine, aminoimidazole-4-carboxamide riboside, and N6-mercaptopurine riboside. Evidence for involvement of amp-activated protein kinase. *J Biol Chem.* 1998;273:23758-23763.

12. Xing Y, Musi N, Fujii N, Zou L, Luptak I, Hirshman MF, Goodyear LJ, Tian R. Glucose metabolism and energy homeostasis in mouse hearts overexpressing dominant negative alpha2 subunit of AMP-activated protein kinase. *J Biol Chem.* 2003;278:28372-28377.

13. Russell RR, 3rd, Li J, Coven DL, Pypaert M, Zechner C, Palmeri M, Giordano FJ, Mu J, Birnbaum MJ, Young LH. AMP-activated protein kinase mediates ischemic glucose uptake and prevents postischemic cardiac dysfunction, apoptosis, and injury. *J Clin Invest.* 2004;114:495-503.

14. Horman S, Beauloye C, Vertommen D, Vanoverschelde JL, Hue L, Rider MH. Myocardial ischemia and increased heart work modulate the phosphorylation state of eukaryotic elongation factor-2. *J Biol Chem.* 2003;278:41970-41976.

15. Wu H, Yang JM, Jin S, Zhang H, Hait WN. Elongation factor-2 kinase regulates autophagy in human glioblastoma cells. *Cancer Res.* 2006;66:3015-3023.

16. Liang J, Shao SH, Xu ZX, Hennessy B, Ding Z, Larrea M, Kondo S, Dumont DJ, Gutterman JU, Walker CL, Slingerland JM, Mills GB. The energy sensing LKB1-AMPK pathway regulates p27(kip1) phosphorylation mediating the decision to enter autophagy or apoptosis. *Nat Cell Biol.* 2007;9:218-224.

17. Dyck JR, Lopaschuk GD. AMPK alterations in cardiac physiology and pathology: enemy or ally? *J Physiol.* 2006;574:95-112.

Figure 1

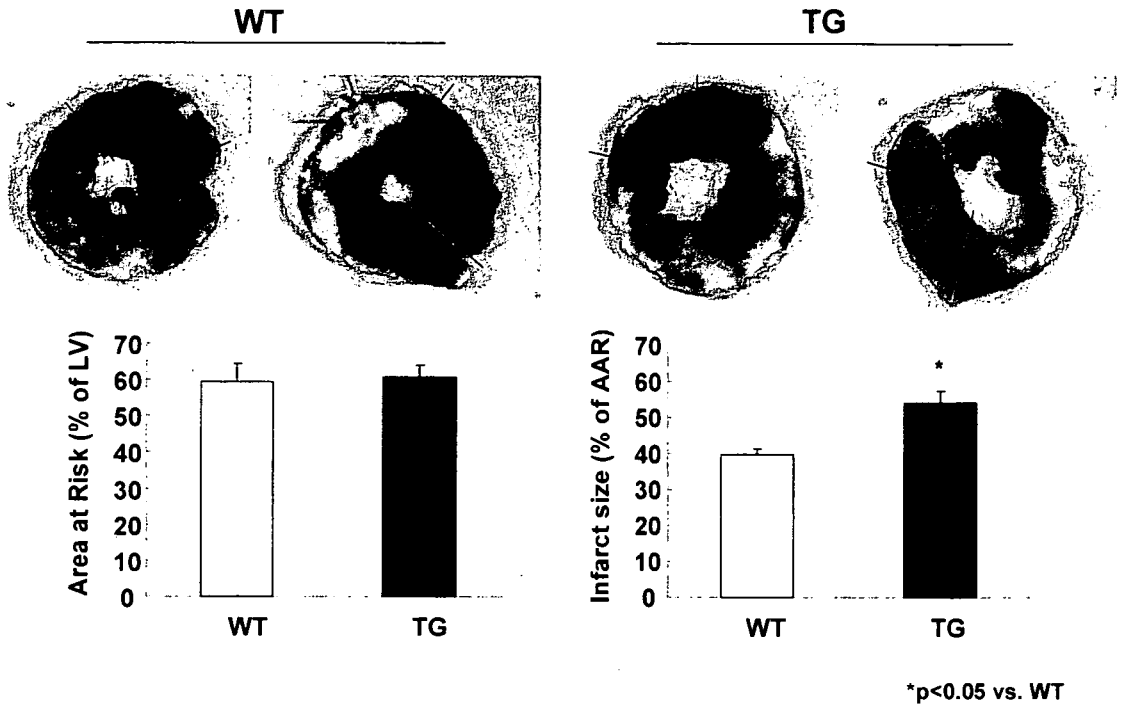

Figure 1 The effect of prolonged ischemia on the size of myocardial infarction in wild type (WT) (n=3) and DN-AMPK (TG) (n=3) mice. The mice were subjected to 90 min of ischemia. Area at risk (left) and the size of the myocardial infarction (right) were determined by Alcian Blue dye and TTC staining, respectively. The detailed method has been described previously [4]. Note that the size of the myocardial infarction was greater in DN-AMPK mice ($p<0.05$) compared to WT.

Figure 2

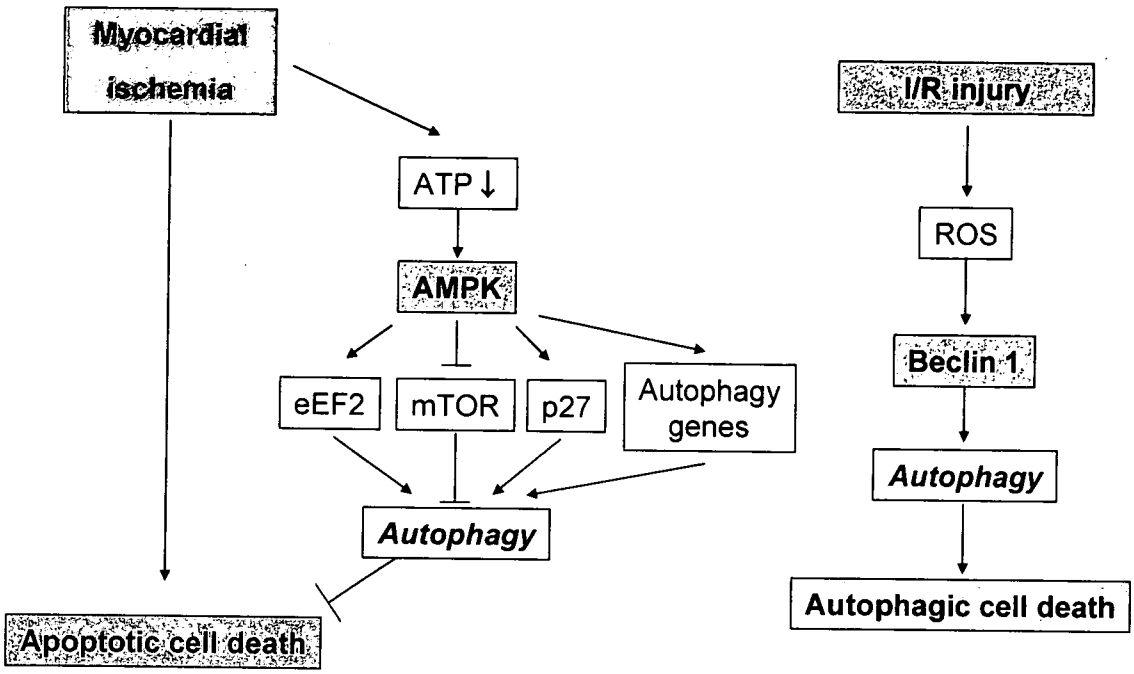

Figure 2 Schematic representation of a model of autophagy induced by myocardial ischemia or ischemia/reperfusion (I/R) injury in the heart. AMPK AMP activated protein kinase, eEF2 eukaryotic elongation factor-2, mTOR mammalian target of rapamycin, ROS reactive oxygen species. ↓ indicates stimulatory whereas ⊥ inhibitory.

MOLECULAR AND CELLULAR BIOLOGY, Apr. 2007, p. 2548–2561 Vol. 27, No. 7
0270-7306/07/$08.00+0 doi:10.1128/MCB.00992-06

Calpain 6 Is Involved in Microtubule Stabilization and Cytoskeletal Organization▽†

Kazuo Tonami,[1] Yukiko Kurihara,[1] Hiroyuki Aburatani,[2] Yasunobu Uchijima,[1] Tomoichiro Asano,[3] and Hiroki Kurihara[1]*

Department of Physiological Chemistry and Metabolism, Graduate School of Medicine, The University of Tokyo, 7-3-1 Hongo, Bunkyo-ku, Tokyo 113-0033, Japan[1]; Genome Science Division, Research Center for Advanced Science and Technology, The University of Tokyo, 4-6-1 Komaba, Meguro-ku, Tokyo 153-8904, Japan[2]; and Department of Biomedical Chemistry, Hiroshima University Graduate School of Biomedical Sciences, Kasumi 1-2-3, Hiroshima 734-8551, Japan[3]

Received 5 June 2006/Returned for modification 11 July 2006/Accepted 21 December 2006

The calpains are a family of Ca^{2+}-dependent cysteine proteases implicated in various biological processes. In this family, calpain 6 (Capn6) is unique in that it lacks the active-site cysteine residues requisite for protease activity. During the search for genes downstream of the endothelin 1 (ET-1) signaling in pharyngeal-arch development, we identified Capn6. After confirming that the expression of Capn6 in pharyngeal arches is downregulated in ET-1-null embryos by in situ hybridization, we investigated its function. In Capn6-transfected cells, cytokinesis was retarded and was often aborted to yield multinucleated cells. Capn6 overexpression also caused the formation of microtubule bundles rich in acetylated α-tubulin and resistant to the depolymerizing activity of nocodazole. Green fluorescent protein-Capn6 overexpression, immunostaining for endogenous Capn6, and biochemical analysis demonstrated interaction between Capn6 and microtubules, which appeared to be mainly mediated by domain III. Furthermore, RNA interference-mediated Capn6 inactivation caused microtubule instability with a loss of acetylated α-tubulin and induced actin reorganization, resulting in lamellipodium formation with membrane ruffling. Taken together, these results indicate that Capn6 is a microtubule-stabilizing protein expressed in embryonic tissues that may be involved in the regulation of microtubule dynamics and cytoskeletal organization.

The calpains are a family of intracellular cysteine proteases whose activities are highly dependent on Ca^{2+} ions (9, 11, 16, 35, 36, 38). Fourteen members of the calpain family are known in mammals, whereas a large number of molecules with structural similarity have been reported to constitute a superfamily beyond species. Calpain 1 (Capn1) (μ-calpain) and Capn2 (m-calpain) are the representative members most extensively studied. They heterodimerize with a small regulatory subunit, Capn4. These "classical" calpains are ubiquitously expressed and are implicated in various cellular functions, such as migration, apoptosis, cell growth, and cell cycle progression. p94/Capn3 is a skeletal-muscle-specific calpain whose loss-of-function mutation causes limb girdle muscular dystrophy type 2A (11, 16, 35). Capn10 has been identified as a molecule associated with an increased risk for type 2 diabetes (11, 16). To date, many proteins have been proposed as candidates for their enzymatic substrates, although the physiologically relevant substrates remain largely unknown (11).

Many large-molecule calpains share a common four-domain structure consisting of domains I to IV (9, 11, 16, 35, 36, 38). Domain II is divided into subdomains IIa and IIb, which generate a substrate-binding cleft between them. The crystal structure of Capn2 has revealed that the cysteine residue in subdomain IIa and the histidine and asparagine residues in subdomain IIb form a catalytic triad (13, 30, 37). Domain III is related to the C2 domain, a Ca^{2+}- and phospholipid-binding module (33). Domain IV is characterized by the presence of multiple EF-hand motifs in Capn1, -2, -3, -8, -9, -11, and -12, whereas other calpains have distinct structures in their C-terminal regions. In Capn5 and Capn6, the C-terminal structure is defined as the T domain, based on homology to *Caenorhabditis elegans* TRA-3, a nematode sex determination factor (35), but the function of this domain is unclear.

In the calpain family, Capn6 is unique in that it lacks the active-site catalytic cysteine residue and may not be a proteolytic enzyme (4). *Capn6* is located on the X chromosome and is expressed during embryogenesis (4, 5, 26). In particular, the mandibular arch, somite and developing skeletal muscle, heart, epithelial border of the fourth ventricle, lobar bronchi, capsule of the lung and kidney, and chorionic plate of the placenta highly express *Capn6* from the mid- to late-embryonic stages (5). In contrast, *Capn6* expression appears to be downregulated after birth (5). These findings led us to postulate some important roles for Capn6 in embryonic development; however, no functional characterization has been reported for Capn6.

Various developmental processes are controlled by genetic hierarchies involved in interactions among different cell populations. In mandibular-arch development, endothelin 1 (ET-1), a 21-amino-acid peptide originally identified as a vascular-endothelium-derived vasoconstrictor (25, 42), has emerged as a regulator of the dorsoventral axis patterning through the

* Corresponding author. Mailing address: Department of Physiological Chemistry and Metabolism, Graduate School of Medicine, University of Tokyo, 7-3-1 Hongo, Bunkyo-ku, Tokyo 113-0033, Japan. Phone: 81-3-5841-3498. Fax: 81-3-5684-4958. E-mail: kuri-tky@umin.ac.jp.

† Supplemental material for this article may be found at http://mcb.asm.org/.

▽ Published ahead of print on 8 January 2007.

induction of *Dlx5* and *Dlx6*, homeobox genes belonging to the vertebrate *Distal-less* homologues (2, 7, 19, 21, 22, 29). However, key molecules downstream of this genetic hierarchy controlling pharyngeal-arch development remain largely unknown. While exploring such downstream genes by microarray analysis, we encountered Capn6 as a candidate molecule. Its expression pattern in the pharyngeal arch and unique molecular form among the calpain family members inclined us to pursue its role in pharyngeal-arch development. To start with, we decided to unveil the molecular function of this molecule. Here, we demonstrate that Capn6 is a microtubule-stabilizing protein. Capn6 overexpression causes a failure of cytokinesis, leading to the formation of multinucleated cells. Immunocytochemical and biochemical analyses revealed the association of Capn6 with microtubules, which appeared to be mediated by domain III. In addition, RNA interference (RNAi)-mediated Capn6 inactivation resulted in a loss of stable microtubules and induced actin reorganization, resulting in lamellipodium formation with membrane ruffling. These results suggest that Capn6 may be involved in the regulation of microtubule stability and actin organization. During pharyngeal-arch development, Capn6 may act as a downstream molecule of ET-1 signaling through its effect on cytoskeletal organization.

MATERIALS AND METHODS

Microarray analysis. Total RNA was extracted from excised embryonic day 10.5 (E10.5) mandibular arches of *ET-1*$^{-/-}$ embryos with ISOGEN (Nippon Gene). Each cDNA sample was synthesized from the total RNA with a Superscript kit (Clontech) and was hybridized to a GeneChip array containing about 12,500 mouse genes. The hybridized arrays were scanned and analyzed with the Affymetrix GeneChip System. The relative abundance of each gene was estimated from the average difference of intensities. Change was calculated by taking the difference in average differences between the *ET-1*$^{+/\pm}$ (wild-type and homozygous) and *ET-1*$^{-/-}$ samples. The score of increase, decrease, or no change of expression for individual genes was defined on the basis of ranking the difference calls from three intergroup comparisons (3 × 3) as follows: no change = 0, marginal increase/decrease = 1/−1, and increase/decrease = 2/−2. The final rank was assigned by summing up the nine values corresponding to the difference calls, and the values varied from −18 to 18. The cutoff value for the final determination of increase/decrease was set as 9/−9.

Plasmids. The 3′ untranslated region of *Capn6* was amplified by reverse transcription (RT)-PCR of cDNA samples from E10.5 mandibular arches and subcloned into the pCRII TOPO vector (Invitrogen) for the generation of antisense riboprobes. For the expression of green fluorescent protein (GFP) fusion protein, the *Capn6* open reading frame and its PCR-amplified deletion mutants were subcloned in frame into the pEGFP-C2 expression vector (Clontech). Wild-type Capn6 expression vectors were constructed by cutting out the GFP gene from pEGFP-Capn6 expression plasmids. For the glutathione *S*-transferase (GST) fusion protein, *Capn6* and its deletion mutants were subcloned in frame into the PGEX-4T-1 vector (Amersham). All of the constructs were verified by sequencing.

Whole-mount in situ hybridization. The *ET-1*$^{-/-}$ mouse was described previously (20). Embryos were harvested at E10.5 and fixed in 4% paraformaldehyde–phosphate-buffered saline (PBS). Whole-mount in situ hybridization was performed as described by Wilkinson using a digoxigenin-labeled *Capn6* riboprobe (41).

Generation of Capn6 antibody. Polyclonal antibody against mouse Capn6 was generated at Transgenic Inc. by injecting a rabbit with a keyhole limpet hemocyanin-conjugated synthetic oligopeptides corresponding to the C-terminal domain of Capn6 (amino acids 605 to 617). The bleeds were affinity purified using Affi-Gel 10 gel (Bio-Rad) coupled with the oligopeptides.

Cell culture and transfection. NIH 3T3, HeLa, and HEK 293T cells were cultured in Dulbecco's modified Eagle's medium containing 10% fetal calf serum and antibiotics at 37°C in 5% CO_2. For transfection, cells were grown to 50 to 90% confluence and were treated with a mixture of plasmid DNA and LipofectAMINE PLUS or LipofectAMINE 2000 reagent (Invitrogen). After 2 to 3 h of incubation, the cells were refed with medium containing fetal calf serum and were allowed to recover for 24 to 48 h. Cells transfected with plasmids encoding GFP derivatives were observed by fluorescence microscopy. For stable transformants of GFP-tubulin, linearized pEGFP-Tub vector (BD Biosciences) was transfected into NIH 3T3 cells and selected with G418. Several independent clones were picked up, and expression was confirmed by fluorescence microscopy and Western blotting.

Immunofluorescence microscopy. Cells were washed with preincubated general tubulin buffer (GTB) {80 mM PIPES [piperazine-*N*,*N*′-bis(2-ethanesulfonic acid)], pH 7, 1 mM $MgCl_2$, 1 mM EGTA} at 37°C, fixed with 4% paraformaldehyde in GTB, permeabilized with 0.2% Triton X-100 in GTB, and washed with GTB at room temperature. After being blocked with 5% skim milk in GTB, the cells were incubated with primary antibodies as follows; the rabbit polyclonal anti-Capn6 antibody, rabbit polyclonal anti-GFP antibody (MBL), and mouse monoclonal anti-α-tubulin and anti-acetylated α-tubulin antibodies (Sigma). Then, the cells were washed and stained with the secondary antibodies (fluorescein isothiocyanate- or rhodamine-conjugated donkey anti-mouse or rabbit immunoglobulin G; Jackson Immunoresearch). For actin staining, 2.5 units/ml rhodamine-phalloidin (Invitrogen) was added to the reaction buffer containing fluorescein isothiocyanate-conjugated secondary antibody. The cells were viewed using a fluorescence microscope (Nikon TE300) or a confocal microscope (Nikon D-ECLIPSE C1). Three-dimensional views (see Fig. 3F and G) were produced from 28 images in a two-dimensional Z stack spanning about 0.15 μm of the center of a single cell using EZ-C1 2.30 (Nikon) software.

Time-lapse video microscopy. Cells were grown on 35-mm culture dishes set in a control chamber maintained at 5% CO_2-95% air at 37°C. Cell images were obtained from 12 to 16 h after transfection at 5-min (for GFP-Capn6 overexpression experiments) or 1-min (for RNAi experiments) intervals on a TE300 microscope (Nikon) using a 20× Nikon objective lens (numerical aperture, 0.45) and an ORCA 100 cooled charge-coupled-device camera (Hamamatsu) and analyzed by AquaCosmos imaging software (Hamamatsu).

Western blotting. For whole-cell lysate preparation, cells were solubilized in PBS containing 1% Triton X-100, 0.1% sodium deoxycholate, 0.02% sodium dodecyl sulfate (SDS), 1 mM phenylmethylsulfonyl fluoride, 0.5 mM vanadate, and protease inhibitor cocktail (Sigma). For crude fractionation, cells were suspended in 80 mM PIPES, pH 7.0, 0.1% NP-40, 1 mM $MgCl_2$, 1 mM EGTA, 1 mM phenylmethylsulfonyl fluoride, 0.5 mM vanadate, and protease inhibitor cocktail (Sigma). After incubation for 15 min on ice, the suspension was passed through a 27-gauge syringe needle and centrifuged at 800 × *g* for 5 min at 4°C. The supernatant was saved as the soluble fraction. The pellet was resuspended in PBS containing 1% Triton X-100 and protease inhibitors, sonicated for 10 s, and subjected to protein analysis. The protein concentration was determined using a bicinchoninic acid protein assay kit (Pierce), and equal volumes of proteins were separated by 7.5% SDS-polyacrylamide gel electrophoresis (PAGE) and then electrotransferred to a polyvinylidene difluoride (PVDF) membrane. After being blocked with 5% skim milk in 0.1% Tween 20 in Tris-buffered saline, pH 7.6, the blots were probed with primary antibodies as follows: rabbit polyclonal anti-Capn6 antibody; rabbit polyclonal anti-GFP antibody (MBL); rabbit polyclonal anti-μ-calpain (Capn1) antibody (Sigma); mouse monoclonal anti-α-tubulin, anti-acetylated α-tubulin, and anti-β-actin antibodies (Sigma); and goat polyclonal anti-MAP4 antibody (Santa Cruz). The membranes were then washed with 0.1% Tween 20 in Tris-buffered saline, pH 7.6, and incubated with peroxidase-conjugated anti-rabbit, anti-mouse, or anti-goat immunoglobulin G (DAKO). The signals were detected using the ECL chemiluminescence detection system (Amersham Bioscience).

Microtubule cosedimentation assay. Cells were lysed in 80 mM PIPES, pH 7.0, 1% Triton X-100, 1 mM $MgCl_2$, 1 mM EGTA, 1 mM phenylmethylsulfonyl fluoride, 0.5 mM vanadate, and protease inhibitor cocktail (Sigma) by passing them through a 30-gauge syringe needle. After incubation on ice for 30 min to depolymerize the microtubules, the lysate was centrifuged at 20,000 × g for 80 min at 4°C to remove cellular debris. The supernatant was divided into two tubes, and 20 μM paclitaxel (Taxol) or vehicle (dimethyl sulfoxide [DMSO]) was added to each sample. After incubation for 30 min at 37°C, the reaction mixture was centrifuged at 20,000 × *g* for 40 min at room temperature. The resultant pellets were resuspended in lysis buffer, separated by 7.5% SDS-PAGE, and subjected to Western blotting analysis with whole lysate and supernatants.

Microtubule binding assay on filter paper. GST-fused full-length Capn6 protein was tested for microtubule binding on filter paper according to the method previously described by Nakaseko et al. (28). Briefly, GST-Capn6 fusion proteins were purified from bacterial lysates by using glutathione beads and subjected to SDS-PAGE. Then, the proteins were transferred to a PVDF filter and incubated in 100 mM PIPES, pH 6.9, 2 mM EGTA, 1 mM $MgSO_4$, 0.1% Tween 20, and 5% skim milk, followed by an additional incubation with paclitaxel-stabilized bovine brain microtubules (50 μg/ml; Cytoskeleton Inc.) in the same buffer. The filter

was then washed and immunoblotted with anti-tubulin antibody. Purified MAP2 (Cytoskeleton Inc.) served as a positive control.

GST pull-down assay. For cell lysate preparation, NIH 3T3 cells were solubilized in pull-down buffer (20 mM Tris-HCl, pH 7.6, 1% Triton X-100, 0.25% sodium deoxycholate, 0.25 M NaCl) containing 1 mM phenylmethylsulfonyl fluoride, 0.5 mM vanadate, and protease inhibitor cocktail (Sigma). The solubilized cell lysates were frozen and thawed twice and sonicated 25 times for 10 s each time. Unbroken cells and cellular debris were removed by centrifugation at 20,000 × *g* at 4°C for 10 min. After incubation on ice for 15 min, the lysates were incubated with 20 μM paclitaxel and 1 mM GTP at 37°C for 30 min to stabilize the microtubules. Then, GST fusion proteins bound to the beads were mixed with lysates and incubated at 4°C for 6 h. The beads were washed three times with pull-down buffer containing protease inhibitors, and the bound proteins were eluted by adding 2.5× sample buffer and then boiled for 5 min. These samples were subjected to 10% (vol/vol) SDS-PAGE, and proteins were detected by Western blotting with anti-α-tubulin or anti-acetylated α-tubulin antibodies. The amounts of GFP fusion proteins were grossly estimated by Ponceau staining.

siRNA experiments. Two different stealth small interfering RNA (siRNA) duplexes designated no. 1298 and 1715, which targeted nucleotides 1298 to 1322 and 1715 to 1739 of the mouse Capn6 mRNA sequence, respectively, and control siRNA containing the same nucleotides as no. 1298 but with scrambled sequence were synthesized by Invitrogen. The sense sequences of 1298, 1715, and control siRNAs were 5′-GGUUCCGUCUUCACCAUCUGUAUAU-3′, 5′-GGACCA CUGACAUUCCUAUUAUCAU-3′, and 5′-GGUUGCUUCCACUACGUCA UUCUAU-3′, respectively. The siRNAs were transfected into NIH 3T3 cells using OligofectAMINE (Invitrogen) according to the manufacturer's protocol. In some experiments, GFP-tubulin-expressing NIH 3T3 cells were used. The efficiency of gene knockdown was evaluated by RT-PCR with primers specific for the mouse *Capn6* mRNA (sense, 5′-GAATGTGGACATCCTACATG-3′; antisense, 5′-GCTGTCCTATTACTGAATAG-3′) and Western blotting. Expression of glyceraldehyde-3-phosphate dehydrogenase (GAPDH) and β-actin served as internal controls for RT-PCR and Western blotting, respectively.

RESULTS

Endothelin-1-dependent *Capn6* expression in pharyngeal-arch development. To explore target genes downstream of the ET-1 signaling involved in pharyngeal-arch development, we performed oligonucleotide microarray analysis on E10.5 *ET-1*$^{-/-}$ and *ET-1*$^{+/\pm}$ mandibular arches to identify genes downstream of the ET-1 signaling in mandibular-arch development. Among 132 genes with decreases in the E10.5 *ET-1*$^{-/-}$ mandibular arch in comparison to the *ET-1*$^{+/\pm}$ control (data not shown), *Capn6* was found to be decreased by ~2.8-fold.

To confirm the downregulation of *Capn6* in the *ET-1*$^{-/-}$ mandibular arch, we performed whole-mount in situ hybridization. *Capn6* expression was detected in the mandibular arch, heart, limb buds, and somites during embryogenesis, suggesting its tissue-specific role during embryonic development (Fig. 1A and C). In the *ET-1*$^{-/-}$ mutant, *Capn6* expression was downregulated in the mandibular-arch mesenchyme, whereas its expression in the most dorsal mandibular epithelium was preserved (Fig. 1B and D). *Capn6* expression in other regions was not affected in the *ET-1*$^{-/-}$ mutant (Fig. 1B).

Capn6 induces multinucleation by interfering with cytokinesis. To characterize the function of Capn6, we fused Capn6 to GFP and overexpressed it in HeLa cells. Among cells transfected with GFP-Capn6, ~20% became bi- or trinucleated 48 h after transfection, whereas only ~3% of control GFP-transfected cells became multinucleated (Fig. 2A to C). Overexpression of wild-type Capn6 also induced multinucleation with comparable frequency (data not shown), suggesting that this effect was not due to GFP fusion. When HEK 293T cells were transfected, almost all Capn6-transfected cells became multinucleated within 7 to 10 days, sometimes with ~10 nuclei (data not shown).

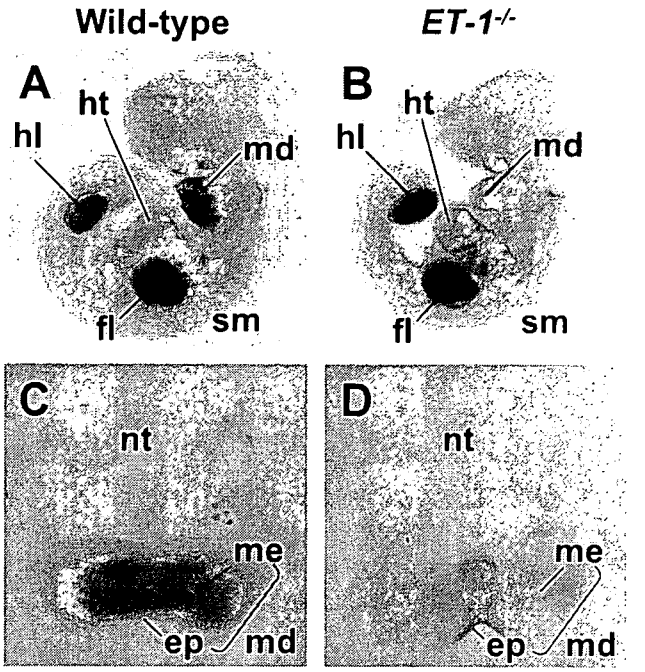

FIG. 1. Expression of *Capn6* in mouse embryos. Whole-mount in situ hybridization was performed on E10.5 wild-type (A and C) and *ET-1*$^{-/-}$ (B and D) embryos using the *Capn6* probe. Whole bodies (A and B) and excised mandibular arches (C and D) are shown. *Capn6* is normally expressed in the mandibular arches, heart, and limb buds. In the *ET-1*$^{-/-}$ mutant, the expression of *Capn6* in the mandibular arches is specifically downregulated, whereas *Capn6* expression in other regions is not affected. ep, epithelium; fl, forelimb bud; hl, hindlimb bud; ht, heart; md, mandibular arch; me, mesenchyme; nt, neural tube; sm, somites.

To explore the cause of the multinucleation induced by Capn6, we followed the fate of Capn6-transfected HeLa cells under time-lapse video microscopy. In all the control GFP-expressing cells examined (n = 13), the cleavage furrow started to ingress within 5 min and daughter cells flattened out within 30 min after the onset of anaphase (Fig. 2D; see Video S1 in the supplemental material). Thereafter, the cytoplasmic bridge disappeared within 90 min (Fig. 2D). Among GFP-Capn6-expressing mitotic cells examined (n = 15), 12 cells were able to complete cell division eventually, but the progression of furrow ingression was obviously retarded in 10 of the 12 cells (Fig. 2E; see Video S2 in the supplemental material). Eight of 12 daughter pairs retained a peanut-shaped morphology at 90 min after anaphase onset, whereas 2 daughter pairs were still tethered to each other with the cytoplasmic bridge beyond 90 min. The other two cells, in which GFP signals were relatively low, showed no apparent retardation of cytokinesis (data not shown). In 3 of 15 cells examined, GFP-Capn6 overexpression caused regression of the cleavage furrow at various time points to yield binucleated cells (Fig. 2F; see Video S3 in the supplemental material). All the Capn6-overexpressing cells commenced mitosis and cytokinesis apparently normally, with the cleavage furrow being appropriately positioned (Fig. 2E and F; see Video S4 in the supplemental material) indicating that Capn6 does not affect the onset of anaphase and cleavage furrow formation. Instead, Capn6 overexpression can disrupt

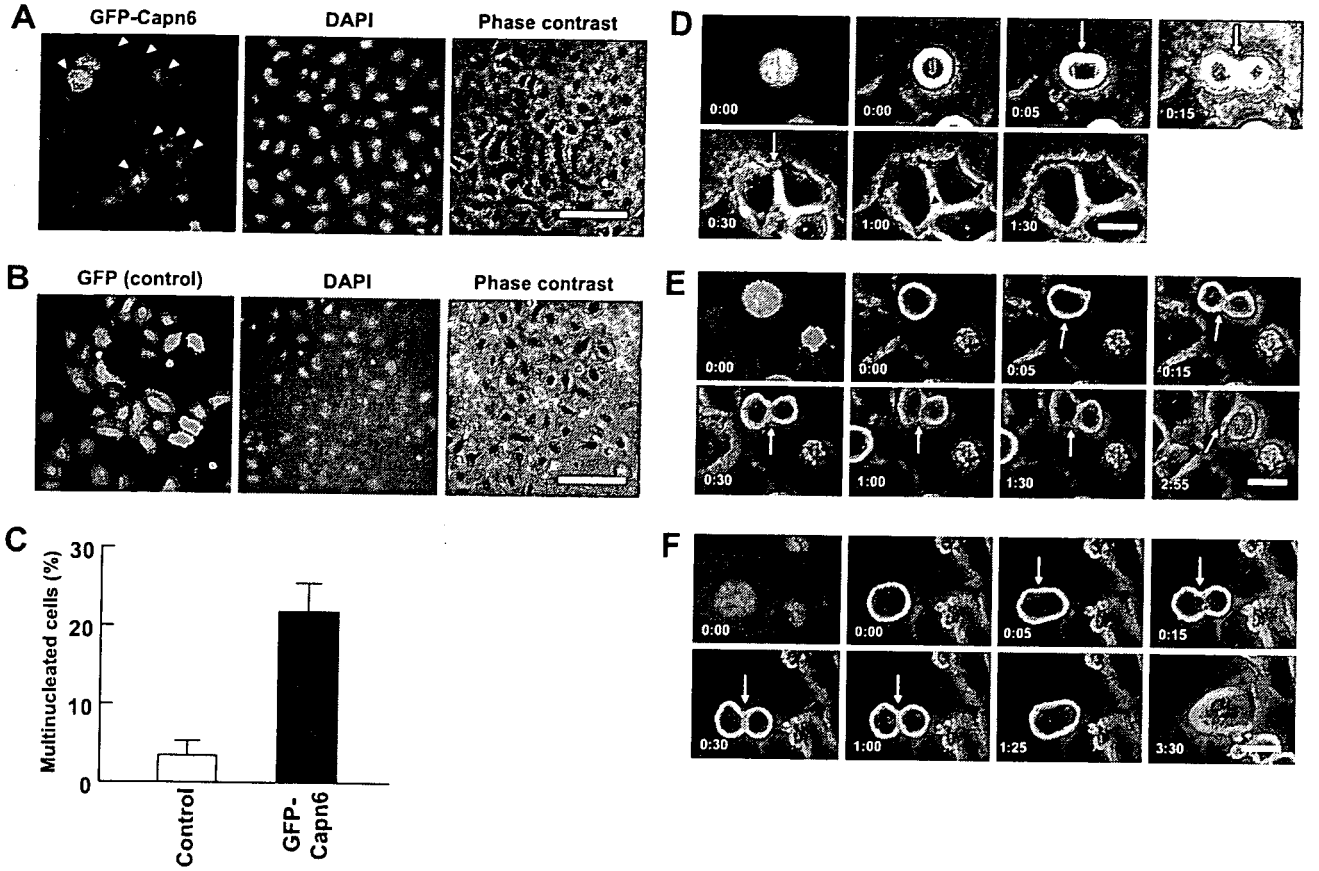

FIG. 2. GFP-Capn6 overexpression impairs cytokinesis and causes the formation of multinucleated cells. (A and B) Multinucleation of HeLa cells by GFP-Capn6 overexpression. Many GFP-Capn6-transfected cells become binucleated (arrowheads) 48 h after transfection (A), whereas most control GFP-transfected cells are mononucleated (B). The scale bars indicate 100 μm. (C) Comparison of multinucleated-cell numbers between control and GFP-Capn6-transfected cells 48 h after transfection. The data represent the mean and standard deviation of four independent experiments. (D to F) Representative images from time-lapse recordings of HeLa cells transiently expressing GFP (D) or GFP-Capn6 (E and F). (D) In control GFP-expressing cells, the cleavage furrow (arrows) started to ingress within 5 min and daughter cells flattened out within 30 min after the onset of anaphase. The cytoplasmic bridge (arrowhead) disappeared within 90 min. (E) In many GFP-Capn6-expressing cells, furrow formation started normally, but its progression was retarded. (F) In some cases, GFP-Capn6 overexpression caused regression of the cleavage furrow to yield binucleated cells. Time is in h/min after anaphase onset (0:00 time point). The scale bars indicate 20 μm.

the progression and completion of cytokinesis, often leading to the formation of multinucleated cells.

GFP-Capn6 colocalizes to and stabilizes the microtubule network. The failure of cytokinesis in Capn6-overexpressing cells led us to speculate that Capn6 may associate with cytoskeletal proteins involved in cytokinesis. To investigate this possibility, we examined the intracellular distribution of GFP-Capn6. In contrast to the diffuse distribution of control GFP protein throughout the cytoplasm and nucleus (Fig. 3A and F and 4A), GFP-Capn6 was mainly distributed in the perinuclear region in HeLa cells (Fig. 3B and G) or in a fascicular pattern in NIH 3T3 cells (Fig. 4C). Costaining with anti-tubulin antibody revealed that these distributions largely overlapped with thick microtubule bundles, whose formation appeared to be facilitated by Capn6 overexpression (Fig. 3B and 4C).

During mitosis, GFP-Capn6 was distributed in association with the mitotic spindle (Fig. 3C). At telophase, GFP-Capn6 was most intensely colocalized to microtubules in the central spindle (Fig. 3D). This colocalization was sustained in the midbody toward the end of cytokinesis, although a large portion of the GFP signals appeared to be distributed throughout the cytoplasm (Fig. 3E).

To determine the nature of microtubule bundles induced by Capn6 overexpression, we examined the level of tubulin acetylation, a posttranslational modification characteristic of stable microtubules (32). Immunostaining with specific antibody revealed that microtubules in GFP-Capn6-overexpressing cells contained high levels of acetylated α-tubulin (Fig. 3G), whereas cells expressing GFP alone did not (Fig. 3F). In particular, the distribution of acetylated α-tubulin corresponded to Capn6-induced microtubule bundles in the perinuclear region in many transfected HeLa cells (Fig. 3G).

To confirm the increase in acetylated α-tubulin by Capn6, immunoblotting was performed on GFP- and GFP-Capn6-transfected HeLa cells. Acetylated α-tubulin levels were increased in GFP-Capn6-transfected cells compared to GFP-transfected cells, whereas total α-tubulin levels were not increased (Fig. 3H). Paclitaxel, a microtubule-stabilizing agent,

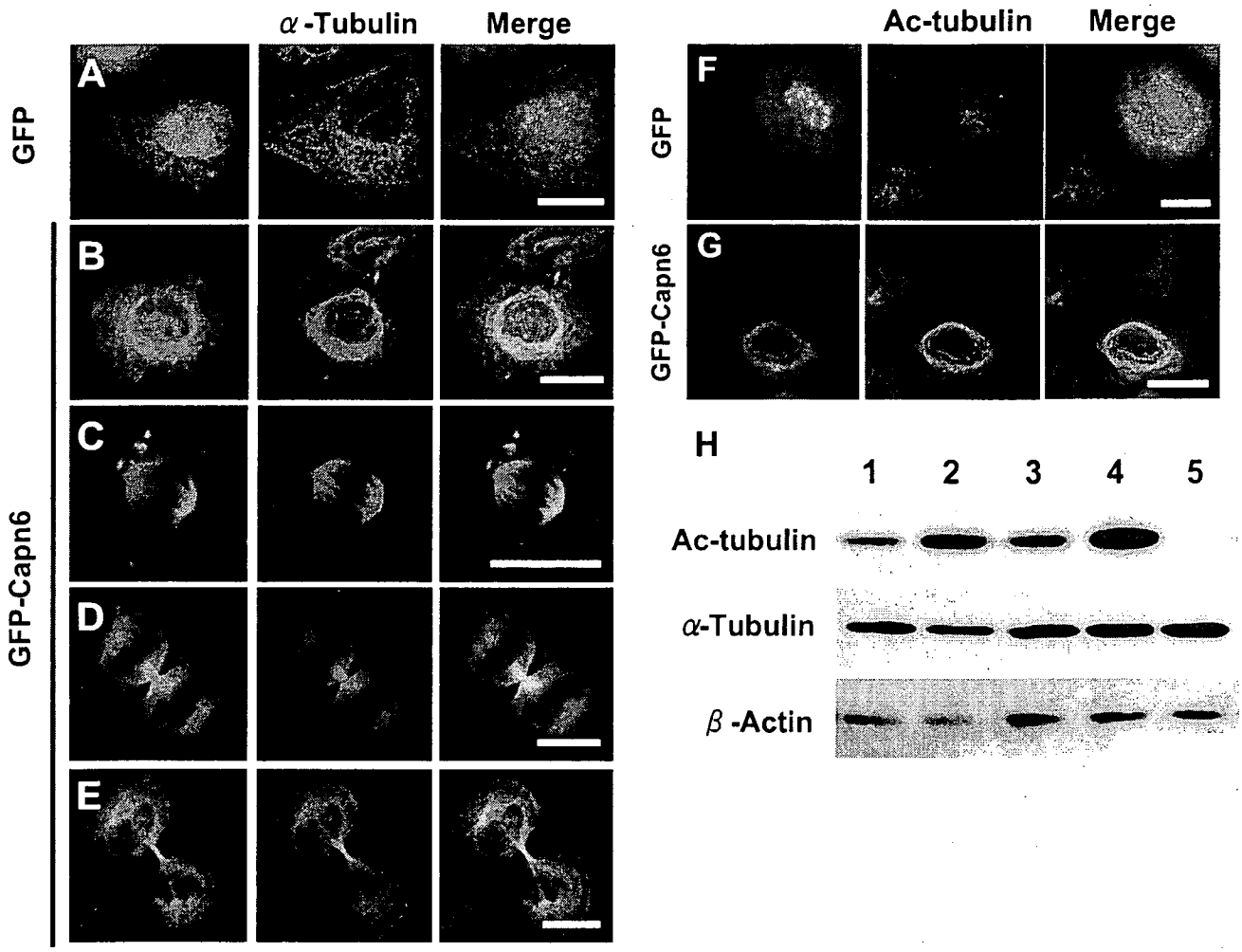

FIG. 3. Subcellular localization of GFP-Capn6 in HeLa cells at various stages of the cell cycle and its stabilizing effect on microtubules. (A to G) Cells were transfected with expression plasmids containing GFP (A and F) or GFP-Capn6 (B to E and G). After 24 h, the cells were stained with the anti-GFP antibody and anti-α-tubulin (A to E) or anti-acetylated α-tubulin (F and G) antibody. Notably, perinuclear microtubule bundling was observed in GFP-Capn6-transfected cells at interphase (B). During mitosis, GFP-Capn6 was distributed in association with the mitotic spindle (C). At telophase, GFP-Capn6 colocalized to the central spindle (D). At the late stage of cytokinesis, GFP-Capn6 colocalized to the midbody, whereas a large portion of the GFP signals were distributed throughout the cytoplasm (E). Three-dimensional Z-stack images show that the acetylated α-tubulin contents (Ac-tubulin), especially in the perinuclear region, were increased in GFP-Capn6-transfected cells (F and G). The scale bars indicate 20 μm. (H) HeLa cells were transfected with GFP (lane 1) or GFP-Capn6 (lane 2), lysed 16 h after transfection, and blotted with anti-acetylated α-tubulin, anti-α-tubulin, and anti-β-actin antibodies. HeLa cells were treated with DMSO (lane 3), 500 nM paclitaxel (lane 4), or 5 μM nocodazole (lane 5) for 1 h and blotted similarly to serve as controls for changes in acetylated α-tubulin levels. Acetylated-α-tubulin levels were increased in GFP-Capn6-transfected cells compared with GFP-transfected cells, whereas total α-tubulin levels were not increased. Blotting for β-actin served as an internal control. Similar results were obtained in three independent experiments. Representative data are shown.

and nocodazole, a microtubule-disrupting agent, induced increase and decrease in acetylated α-tubulin levels, respectively (Fig. 3H), indicating that the increase in acetylated α-tubulin in GFP-Capn6-transfected cells may reflect increased stability of microtubules.

In addition, the stability of microtubule bundles was tested by treatment with low-dose nocodazole. In cells expressing GFP alone, the microtubule network was largely disrupted by 500 nM nocodazole (Fig. 4A and B). In contrast, microtubule bundles induced by GFP-Capn6 were resistant to 500 nM nocodazole (Fig. 4C and D). These results indicate that Capn6-induced microtubule bundling is likely due to increased stability of microtubules.

Capn6 is a calpain family member that lacks active-site cysteine and histidine residues critical for proteolysis. It is therefore unlikely that the microtubule-stabilizing effect of Capn6 is mediated by protease activity common to other calpains. Indeed, the calpain inhibitors E-64 and Z-LLal did not inhibit the Capn6-induced formation of microtubule bundles (data not shown).

Endogenous Capn6 associates with microtubules. To further characterize the nature of Capn6, we raised a polyclonal